A Neural Network Atmospheric Model for Hybrid Coupled Modelling

by

Youmin Tang, William W. Hsieh, Benyang Tang

Oceanography/EOS

University of British Columbia, Vancouver, B.C., Canada V6T 1Z4

Keith Haines

Department of Meteorology, University of Edinburgh

The King's Buildings, Edinburgh EH9 3JZ, United Kingdom

February 18, 1999

Submitted to Climate Dynamics

Abstract

The possibility of using a nonlinear empirical atmospheric model for hybrid coupled atmosphere-ocean modelling has been examined with a neural network (NN) model for predicting the contemporaneous wind stress field from the upper ocean state. Upper ocean heat content (HC) from a 6-layer ocean model was a better predictor of the wind stress than the (observed or modelled) sea surface temperature (SST). Our results showed that the NN model generally had slightly better skills in predicting the contemporaneous wind stress than the linear regression (LR) model in the off-equatorial tropical Pacific and in the eastern equatorial Pacific. When the wind stresses from the NN and LR models were used to drive the ocean model, slightly better SST skills were found in the off-equatorial tropical Pacific and in the eastern equatorial Pacific when the NN winds were used instead of the LR winds. Better skills for the model HC were found in the western and central equatorial Pacific when the NN winds were used instead of the LR winds. Why NN failed to show more significant improvement over LR in the equatorial Pacific for the wind stress and SST is probably because the relationship between the surface ocean and the atmosphere in the equatorial Pacific over the seasonal time scale is basically linear.

1 Introduction

Within the last decade, many models have been developed for forecasting the El Niño-Southern Oscillation (ENSO) phenomena, a coupled atmosphere-ocean interaction centred in the tropical Pacific (Barnston et al., 1994 and Latif et al., 1994). These models are generally classified into three groups: dynamical coupled models, statistical models and hybrid coupled models.

A hybrid-coupled model (HCM) connects a statistical atmospheric model to a dynamical ocean model (Latif and Villwock 1990; Neelin 1990; Barnett et al. 1993; Balmaseda et al. 1994). This design uses the fact that the ocean has the long-term memory in the

coupled atmosphere-ocean system. The fast adjustment of the atmosphere to the ocean variables such as the sea surface temperature (SST) and upper ocean heat content (HC) motivates the use of a steady-state statistical model for the atmosphere. All HCMs are based on the assumption that for monthly or longer time scales, contemporaneous correlation between wind stress and oceanic variables is associated with the atmosphere's rapid non-local adjustment to the oceanic anomaly patterns throughout the basin (Syu et al.1995). The main advantages of an HCM are: (1) easier understanding of the coupling mechanisms and lower computing cost than a fully coupled GCM (Blanke et al 1997); (2) performing comparable to or even better than a coupled GCM in simulation and prediction (Palmer et al 1994).

An important aspect affecting the HCM performance is the construction of the empirical atmospheric model, e.g. what method was used for estimating the surface wind stress field from a given ocean state, and which oceanic variables were used as predictors for the wind stress. The methods used have advanced from correlation (Latif and Villwock 1990, Latif and Flügel 1991), linear regression with EOF modes (Barnett et al. 1993) to SVD (Singular Value Decomposition) (Syu et al.1995). However, all empirical atmospheric models used in HCMs have so far been linear statistical models. Hence in this paper, we investigate the possibility of improving the empirical atmospheric model by a nonlinear approach using neural networks. Hsieh and Tang (1998) gave a review on the recent applications of neural network models to prediction and data analysis in meteorology and oceanography.

This paper is structured as follows: Section 2 briefly describes the dynamical ocean model. Section 3 describes the empirical atmospheric models, including linear and nonlinear models. Section 4 compares the wind stress estimated using the linear and nonlinear models. Section 5 compares the the ocean model forced with the wind stress from the two empirical atmospheric models.

2 Ocean Model

The ocean model used in this research is one of intermediate complexity, originated from Anderson and McCreary (1985) and Balmaseda et al. (1994, 1995), but extended to six active layers in this study. It consists of depth averaged primitive equations in six active layers, overlying a deep inert layer. The model allows for an exchange of mass, momentum and heat at each layer interface by a parameterisation of entrainment. It has been shown to be a useful tool for studying the ENSO problem and can compare favourably with much more elaborate GCMs (Palmer and Anderson 1994)

The model equations and parameterisations are shown in the Appendix. The model uses an Arakawa C grid layout, with a resolution of 1.5° x 1.5°, covering an extension from 30°N - 30°S in latitude and from 123°E - 69°W in longitude. The time step for integration is two hours. The boundaries are closed, with free slip conditions.

The model was first spun up for 100 years with monthly climatological wind stress and heat flux Q_s as forcing fields. The climatological wind stress used consisted of the seasonal mean of the FSU (Florida State University) observed wind stress (Goldenberg and O'Brien 1981), while the heat flux was represented by the Oberhuber (1988) heat flux Q_0 plus a relaxation term to T_0, the observed SST, i.e.

$$Q_s = Q_0 + \lambda(T - T_0), \tag{1}$$

where T is the model SST, Q_0 and T_0 are the monthly climatological heat flux and SST, respectively, and λ (which is negative) controls the rate of relaxation to the observed SST.

After the 100-year spinup by the seasonal forcing, the model seasonal climatology was obtained. We then made a 30-year model control run, with forcing by the FSU wind stress from 1961-1990. The very good performance of the model is seen from the statistics given in the Appendix. Model outputs such as SST and HC can further be used as predictors for the atmospheric model. For this integration the surface heat formulation was modified

to

$$Q_s = Q_0 + \lambda(T_m - T_0) + 0.2\lambda(T - T_m), \tag{2}$$

where T_m represents the model SST climatology. The factor 0.2 allows a weaker relaxation to the model seasonal cycle, so that the model SST anomalies have similar magnitudes to those observed (Stockdale, 1992).

For easier comparison in the following sections, the ocean domain was divided into several standard regions, Niño1-4 and Eq1-3 (Fig.1).

3 Atmospheric models

a EOFs for predictors and predictands

Two empirical atmospheric models were constructed: One was the traditional linear regression (LR) model widely used in HCMs (Barnett et al 1993); the other was a non-linear regression model, by neural networks.

As potential predictors for both atmospheric models, several oceanic variables were chosen, namely the observed SST, the model SST and HC from the ocean model forced with the observed wind stress. The time period taken for the model construction was from 1964-1990, since in the first 3 years, the output of ocean model was greatly affected by the ocean initial conditions and had a poor agreement with observations. The observed SSTs were from the Comprehensive Ocean Atmosphere Data Set.(COADS, Slutz et al 1985). The FSU wind stress was also detrended by Singular Spectral Analysis (Allen,1992) and smoothed with a 3-month running mean filter.

As in other studies (Barnett et al 1993, Balmaseda 1994), an EOF (Empirical Orthogonal Function) analysis was first applied to each dataset to extract the predictors and predictands. The oceanic predictor field $T(\mathbf{x}, t)$, and the predictand field $\tau(\mathbf{x}, t)$, the

zonal or meridional component of the wind stress, were expressed by EOF analysis as

$$T(\mathbf{x},t) = \sum_n \alpha_n(t) e_n(\mathbf{x}) \qquad\qquad \tau(\mathbf{x},t) = \sum_n \beta_n(t) f_n(\mathbf{x}), \tag{3}$$

where n is the mode number and the seasonal cycle had been removed for both fields prior to the EOF analysis. For the model SST and HC, the first 3 EOF modes accounted for over 70% of total variance, whereas for the observed SST about 67% of total variance was explained by the first 3 EOF modes. In contrast, the first 3 wind stress EOFs explained only 35% of the total variance, due to the presence of high frequency oscillations and noise in the wind stress field. The first three wind EOF modes still captured the main low frequent signals, e.g. ENSO and the first wind EOF modes are highly correlated with the observed SST anomaly averaged over the NINO 3 area (not shown).

All variables have a common feature from their EOF analysis, i.e. the variance contribution by individual modes became rather small after the first 3 modes. Hence, following the suggestions of Latif et al (1990) and Goswami and Shukla (1991), we used the first 3 EOF modes of oceanic variables T as predictors, and the first 3 EOF modes of wind stress as predictands, in constructing both the linear and the non-linear models. The linear regression model is similar to that of Barnett et al (1993).

b Neural Network Model

The nonlinear neural network (NN) model used in this study was the feed-forward NN (Hsieh and Tang, 1998, Tangang et al. 1998a,b). The 3 input neurons were the first 3 EOF time series $\alpha_n(t)$ (either for SST or for HC), and the single output neuron was one of the (zonal or meridional) wind stress EOF time series $\beta_n(t)$, i.e. a separate network was used to predict each of the wind stress EOF modes. There was one hidden layer containing 3 neurons lying between the input layer and the output layer. In the case where both SST and HC are used as predictors, the network had 6 input neurons. Note that there was no time lag between the predictors and the predictand.

To alleviate the problems with NN modelling, i.e. overfitting and instability (Hsieh and Tang, 1998), we used an ensemble of 25 NNs with random initial parameters. The final output of the NN model was the ensemble average of the 25 individual model outputs.

A cross-validation procedure was used to measure the prediction skills. The record of 1964-1990 was divided into 3 segments, the first 7 years and the latter two 10-years periods. Two of the data segments were used to train the models, and the third used for testing the model predictions. The segments were rotated, so that testing could be done for the entire record. This design ensured that no training data were used for testing the prediction skills.

4 Results from atmospheric models

a The predictors

So far, almost all HCMs used either simulated SST from ocean models or observed SST to estimate the wind stress (Barnett et al 1993; Syu et al.1995). Whether SST is the best predictor for the wind stress is debatable. Observations showed that the SSTs do not reflect the changing subsurface temperatures in the tropical western Pacific, where subsurface temperature anomalies and thermocline displacements have an important role in the ocean-atmosphere coupling processes, (White and Pazan 1987, Latif and Graham 1992). Therefore, upper ocean heat contents (HC) as predictors might have higher skills than SST.

Upper HC is defined here as the sum of the temperatures over the first two layers, calculated from

$$HC_i = \frac{h_i(T_i - T_7)}{\sum_{i=1}^{6} H_{init}(i)} \qquad HC = \sum_{i=1}^{2} HC_i, \tag{4}$$

where T_7 is the temperature of the bottom layer, and $H_{init}(i)$ is the initial thickness of layer i.

The first EOF modes for the HC, the zonal and meridional wind stress (Fig.2), are the modes associated with the ENSO oscillation– where the HC shifts east-west along the equator (Fig.2a), the zonal wind anomaly develops in the western equatorial Pacific (Fig.2b), and the trade winds show anomalous convergence along the equator (Fig.2c). Because of their ENSO nature, the anomalies in these EOF modes are all mainly confined to within 15°N - 15°S (Fig.2). To explain the anomalies outside this narrow equatorial belt, the second, third, and even higher modes are needed.

Table 1 shows the cross-validated skills attained by the NN and LR models with the observed SST, model HC, model SST, and model SST+HC serving as predictors for the wind stress EOF time series β_n $(n = 1, 2, 3)$. Here $SST + HC$ does not mean a combined EOF, but that their separate EOF time series normalized by the standard deviations are the predictors. HC as predictors generally had the highest skills as expected, whereas both observed SST and model SST generally attained the lowest skills. SST+HC predictors attained lower skills than HC alone. This suggests that the first 3 EOFs of HC have well represented the ocean status, and more SST EOF modes input only bring additional noise and lead to overfitting. For the first zonal stress mode, the model SST actually did better than the observed SST, probably because the ocean model acted as a complicated space-time filter, thereby removing some noise in the SST (Latif and Graham 1992). For the other wind stress modes, the model SST did not do as well as the observed SST. In general, NN did not predict the first zonal or meridional wind stress mode much better than LR; only for the second and third modes did NN seem to have an edge over LR (Table 1).

b Prediction skills of the NN and LR models

Since we only tried to predict the first 3 wind stress modes, the prediction skills were often compared in later sections against the wind stress reconstructed from the first 3 EOF modes of the FSU wind stress, which we will refer to as the idealized wind stress.

Such a comparison more objectively evaluates the skill of the atmospheric model, as it excludes the noisy higher modes which are not modelled. Fig 3 is the correlation map between the idealized wind stress and the FSU wind stress, showing that the idealized field is a reasonable representation, especially in the western and central Pacific.

As the model HC has the best prediction skills for the wind stress, henceforth we will only use the HC as predictor. The reconstructed stress field was obtained using the predicted EOF time series, either from NN or LR, for the first 3 EOF modes. The cross-validated correlation and Root Mean Square (RMS) error of the reconstructed stress field from NN model verified with the idealized field were shown in Fig.4 and Fig.5. As seen in Fig.4, for zonal stress, the best skills occurred at the equatorial western and eastern Pacific, whereas the worst occurred at the coast off South America, the Australian summer monsoon region and the subtropical North Pacific. The high skill areas are associated with the anomalous SST areas during ENSO events where the response of zonal stress to the ocean status is strong due to active coupling. The lower correlation along the coast of South America might be attributed to the fact that wind-stress is almost 'white' in this region (Goldenberg and O'Brien, 1981, Latif and Flügel 1991). For meridional stress, the highest skills were found in the Intertropical Convergence Zone (ITCZ) and the South Pacific Convergence Zone (SPCZ) areas.

The RMS error map (Fig.5) indicated that the estimation of the amplitude by the NN model was good, especially in eastern Pacific ocean. Large RMS errors only occurred at the ITCZ and SPCZ areas, in contrast to the correlation map (Fig.4), where these two areas have good skills (especially for the meridional stress). The active coupling in these areas induced large anomalous variations in the stress, which generated large amplitude errors even though the phase errors were small, producing good correlations but large RMS errors.

Differences between the prediction skills of the NN model and the LR model for the period of 1964-1990 are shown in Figs. 6 and 7. The correlation skill differences (Fig.6)

between NN and LR were very small, though NN skills were indeed slightly ahead of LR skills in most areas. For the zonal stress (Fig.6a), the NN model outperformed LR in almost the whole subtropical domain of 15°N - 30°N and near the Niño3 region. That the improvements occurred in these regions can be understood from our earlier finding (Table 1) that the NN and the LR had the same skill in predicting the mode 1 zonal stress (Fig.2b), and the NN had an edge over LR for modes 2 and 3. Hence only in regions outside the main anomaly area of mode 1 (i.e. the western equatorial Pacific in Fig.2b) would the NN appear to have slightly better skill than LR, as found in Fig.6a. For the meridional stress (Fig.6b), NN did slightly better in the eastern Pacific away from the equator.

The RMS error difference between the two models (Fig.7) indicated that the NN model slightly outperformed the LR model for almost the whole domain except mainly for the western equatorial region of 150°E - 160°W centred at 5°S. The slight advantage of NN over LR is manifested more clearly in the RMS error map (Fig.7) than in the correlation map (Fig.6), suggesting that model nonlinearity may be slightly more useful in estimating the amplitude than in estimating the phase of the wind stress anomalies.

The very small skill differences between NN and LR follows from the fact that the equatorial dynamical system is almost linear, so a nonlinear model does not give much better results than a linear model. Tang et al. (1999) found that with sea level pressure (SLP) as predictors for the SST anomalies, NN slightly outperformed LR in the Niño3 region, but vice versa in the Niño4 region, suggesting that nonlinearity is quite weak in the eastern-central equatorial Pacific, but even weaker in the western-central equatorial Pacific. Here, Fig.7 and to a lesser extent Fig.6 are consistent with the Tang el al. (1999) finding.

5 The ocean model driven by the empirical wind

a SST skills

To assess the effect of the empirical wind stress from the NN and the LR models on the ocean model, we ran the ocean model twice, with forcing by the two model predicted wind stresses during the period 1964-1990. The outputs of the ocean model forced by the idealized wind stress (i.e. the first 3 EOFs of the FSU data) were later used to verify the skills from the empirical wind stress. Fig.8 compares the SST from the ocean model driven by the idealized wind stress with that driven by the full FSU stress, showing a generally close relation, especially in the western and central equatorial Pacific. This justifies the use of the ocean model driven by the idealized stress as the standard for comparing the empirical winds.

Fig.9 shows the skill of the SST from the ocean model forced with the empirical wind stress from the NN model. As seen in the correlation map (Fig.9a), the skill is good, with a correlation of over 0.8 covering much of the whole model domain. The highest skill, up to over 0.9, occurred at the central equatorial Pacific region.

A comparison of the ocean models driven by the empirical wind stress from the NN model and that from the LR model was then made. Fig.10a depicts the difference in the model SST correlation skills between the NN model and the LR model when they were each verified against the standard SST, i.e. the SST from the model driven by the idealized wind stress. For the equatorial western and central Pacific, the difference was negligible. As mentioned earlier, this is probably due to the mainly linear dynamics in the equatorial western and central Pacific. The largest differences occurred in the off-equatorial areas and in the eastern equatorial Pacific, where the NN winds tended to outperform the LR winds. The maximum correlation difference reached 0.34 in the northwest region around 150°E and 15°N. The positive correlation skill areas in the off-equatorial regions of Fig.10a roughly coincided with the positive zonal wind stress skills attained by the NN over LR in

Fig.6a. There was no such agreement between Fig.10a and Fig.6a in the eastern equatorial Pacific, where the skill differences between NN and LR were small for the zonal stress, but relatively large for the SST. This could be due to the fact that in the equatorial western Pacific, the oceanic response is mainly locally forced by the wind stress, whereas in the eastern Pacific, equatorial Kelvin wave propagation, upwelling and vertical mixing are thought to predominantly control the SST variability (Battisti 1988).

The difference in the SST RMS error between the ocean models driven by the NN and LR wind stress (Fig.10b) generally agreed with Fig.10a, i.e. higher correlation skill areas corresponded with lower RMS error regions, and vice versa.

While the above comparisons were based on the model ocean forced with the idealized wind stress as standard, the comparisons based on the model forced with the FSU stress yielded the same conclusions (not shown). We averaged the model SST forced by the FSU stress, the NN and the LR stress over the Niño 1+2 region, and the whole off-equatorial Pacific in the south (25°S - 15°S, 130°E - 80°W) and in the north (15°N - 25°N, 130°E - 80°W) to get the individual SST indices over these areas. With the ocean model driven by the FSU stress as the comparison standard, the correlation skills for the NN model were 0.38, 0.57 and 0.50 respectively in these 3 areas, compared with correlations of 0.31, 0.51 and 0.41 for the LR model in the same areas.

In summary, using a nonlinear empirical atmospheric model to drive the ocean might bring modest benefits for SST simulation in the off-equatorial tropical regions and in the eastern equatorial Pacific. Improvements in the equatorial western and central Pacific would be unlikely as the dynamics in these regions appeared very nearly linear from other studies (e.g. Tang et al. 1999).

b Heat content Skills

The HC redistribution in the western tropical Pacific can lead the evolution of SST anomalies in the eastern Pacific and has been known to be an important factor in the evolution

of many ENSO episodes. In particular, the HC anomalies over the equatorial band 5°N to 5°S can be a very good precursor for the SST anomalies in the Niño3 region (Zebiak 1989, Latif et at 1992, Balmaseda et al 1994). We therefore examined the HC in the ocean model forced with the wind stress from the NN model and from the LR model. The HC from the ocean model forced with the idealized stress was taken as the verification standard.

The HC skill from the ocean forced with the NN model wind stress was generally better than with the LR stress for the western Pacific basin, in particular in the western and central Pacific over the equatorial band of 10°N to 10°S (Fig.11). From the ocean model driven by the idealized stress, the HC anomalies averaged over the whole equatorial Pacific (124°E-70°W,5°N-5°S) led the observed Niño3 SST anomalies by 3-4 months (Fig.12). Their correlations were 0.73 and 0.72 with the HC leading by 3 and 4 months respectively. The 3-month lag correlations of the observed Niño3 SST anomalies and the HC index averaged over whole equatorial Pacific for the ocean model forced by the NN wind and by the LR wind did indicate that the NN wind had slightly better skill (0.62 for NN and 0.58 for LR).

6 Conclusions

We have examined the possibility of using a nonlinear empirical atmospheric model for hybrid coupled modelling, by developing a neural network (NN) model for predicting the contemporaneous wind stress field from the ocean state, and comparing the NN model with a linear regression (LR) model. Upper heat content (HC) from an ocean model was found to be a better predictor of the wind stress than the (observed or modelled) SST. Our results showed that the NN model generally had slightly better skill in predicting the contemporaneous wind stress than the simple LR model in the off-equatorial tropical Pacific and in the eastern equatorial Pacific, mainly through better predictions of the second and third wind stress modes.

When the NN and LR model produced wind stresses were used to drive the ocean model, slightly better SST skill was found in the off-equatorial tropical Pacific and in the eastern equatorial Pacific when the NN winds were used instead of the LR winds. Better skill for the model HC were found in the western and central equatorial Pacific when the NN winds were used instead of the LR winds. Since the HC involves the product of the upper ocean temperature with the thickness of the upper ocean, it is a more nonlinear variable than the SST– this may partly explain why the nonlinear NN model, when compared with the LR model, generally predicted the HC better than the SST. Because changes in the HC in the western equatorial region can lead to SST anomalies in the eastern Pacific, the potential skill improvement for HC by NN could be of interest.

As discussed in Tang et al.(1999), there are several possible reasons why NN failed to show more significant improvements over LR in the equatorial Pacific for wind stress and SST. The first (and the most probable) is that the relation between the surface ocean and the atmosphere in the equatorial Pacific over the seasonal time scale is basically linear, with nonlinear processes playing only minor roles. The linear assumption was also supported by Xue et al (1994).

The second reason is that the data records are not long enough. NN is more capable than LR but the data requirement is also considerably higher. To extract more than the linear rules from the data, longer records of good quality data are needed. As Barnett et al.(1993) built LR models for individual calendar months, we also tested empirical atmospheric models for individual seasons. Although the seasonal approach can include the effect of the different basic states in different seasons of the year, we did not find the overall cross-validated anomaly skill better than the model using all the data– the tradeoff being that by dividing the data record into seasons, we have even less data to construct each seasonal model.

Finally, the NN model is still a rudimentary one and further improvements in the NN model design is possible. So far, the NN has been used as a nonlinear regression model.

Work is underway to develop a NN nonlinear canonical correlation analysis model, which should provide a more optimal connection between the predictor and predictand fields.

7 Appendix: Ocean Dynamical Model

Like the two-layer model of Balmaseda et al (1994), this 6-layer model includes explicit nonlinear thermodynamics for all layers, accounting for horizontal advection, vertical heat transport, diffusion and, in the first layer, surface heat flux. Besides the physical processes considered in the two-layer model, the 6-layer model includes a viscosity between these layers to account for wind driven Ekman effects, simple convective mixing between 2 adjacent layers due to upwelling and horizontal advection.

The model equations are as follows:

$$\left(\frac{\partial}{\partial t} + u_i\frac{\partial}{\partial x} + v_i\frac{\partial}{\partial y} + f\mathbf{k}\wedge\right) h_i\mathbf{u_i} = -\frac{h_i}{\rho_0}\nabla p_i + \mathbf{M_i} + \frac{\tau}{\rho_0} + \nu\nabla^2(h_i\mathbf{u_i}) + \mathbf{V_i}, \tag{5}$$

$$\left(\frac{\partial}{\partial t} + u_i\frac{\partial}{\partial x} + v_i\frac{\partial}{\partial y}\right) h_i = D_i + d\nabla^2 h_i, \tag{6}$$

$$\left(\frac{\partial}{\partial t} + u_i\frac{\partial}{\partial x} + v_i\frac{\partial}{\partial y}\right) T_i = Q_s + H_i + \kappa\nabla^2 T_i, \tag{7}$$

where layer subscript $i = 1, ..., N$. The symbols u and v are the zonal and meridional components of velocity respectively, p is the pressure, h is the layer thickness, τ is the wind stress, T is temperature, f is the Coriolis parameter given by $f = \beta y$, ρ_0 is a constant density, and ν, d and κ are the coefficients of momentum, thickness and heat diffusivity. The terms $D_i, \mathbf{M_i}, H_i$ are the mass, momentum and heat exchanges between layers and are discussed below. The term Q_s is the surface heat flux determined as for the 2-layer model and $\mathbf{V_i}$ is a vertical viscosity used if the Ekman layer is resolved. $\mathbf{V_i}$ is parameterized as

$$\mathbf{V_i} = A_i(\mathbf{u_{i-1}} - \mathbf{u_i}) + A_{i+1}(\mathbf{u_{i+1}} - \mathbf{u_i}), \qquad \text{where} \quad A_{i+1} \leq A_i$$

The pressure gradients are

$$\frac{1}{\rho_0}\nabla p_i = g\alpha\nabla\left(\sum_{j=1}^{i-1} h_j(T_i - T_{N+1}) + \sum_{j=i}^{N} h_j(T_j - T_{N+1})\right) - g\alpha\left(\frac{h_i}{2} + \sum_{j=1}^{i-1} h_j\right)\nabla T_i \quad (8)$$

where g and α are the gravitational constant and the thermal expansion coefficient respectively. The pressure at the sea surface is

$$p_s = -g\rho_{N+1}\left(H_0 - \sum_{j=1}^{N} h_j\right) - g\sum_{j=1}^{N}\rho_j h_j, \quad (9)$$

and H_0 is the total depth of the model (a constant), and ρ_j is the density of the jth layer. D_i is based on the upwelling, ϵ_{ei}, and downwelling, ϵ_{di}, velocities between layers i and $i+1$ which are parameterised as follows:

$$\epsilon_{ei} = (H_i - h_i)^2/t_{ei}H_i, \qquad \text{if} \quad h_i \le H_i \quad \text{else} \quad \epsilon_{ei} = 0, \quad (10)$$

$$\epsilon_{di} = -(H_i - h_i)^2/t_{di}H_i, \qquad \text{if} \quad h_i \ge H_i \quad \text{else} \quad \epsilon_{di} = 0,$$

where H_i is the nominal layer depth towards which entrainment or detrainment tend to force layer i, and t_{ei} and t_{di} are the entrainment and detrainment time scales respectively. The total vertical velocity may therefore be expressed as

$$\epsilon_i' = \frac{1}{2}(\epsilon_{ei} + |\epsilon_{ei}|) + \frac{1}{2}(\epsilon_{di} - |\epsilon_{di}|).$$

The thickness of the ith layer can be changed by mass exchanges at both its top and bottom surfaces, with layer $i-1$ above and $i+1$ below. The total mass exchanged in (6) is given by

$$D_i = \epsilon_i' - \epsilon_{i-1}'.$$

Note that within each layer the parameters only control entrainment or detrainment with the layer below. Any entrainment or detrainment with the layer above is determined by the thickness of the layer above.

The momentum exchanges for layer i are

$$\mathbf{M_i} = \epsilon_i'\mathbf{u_{i+1}} - \epsilon_{i-1}'\mathbf{u_i} \qquad \text{for} \quad \epsilon_i' \ge 0, \epsilon_{i-1}' \ge 0, \quad (11)$$

$$\mathbf{M_i} = \epsilon'_i \mathbf{u_{i+1}} - \epsilon'_{i-1} \mathbf{u_{i-1}} \qquad \text{for} \quad \epsilon'_i \geq 0, \epsilon'_{i-1} \leq 0,$$

$$\mathbf{M_i} = \epsilon'_i \mathbf{u_i} - \epsilon'_{i-1} \mathbf{u_{i-1}} \qquad \text{for} \quad \epsilon'_i \leq 0, \epsilon'_{i-1} \leq 0,$$

$$\mathbf{M_i} = \epsilon'_i \mathbf{u_i} - \epsilon'_{i-1} \mathbf{u_i} \qquad \text{for} \quad \epsilon'_i \leq 0, \epsilon'_{i-1} \geq 0.$$

The heat transport term related to upwelling and downwelling is

$$H_i = -\epsilon'_i \lambda_i (T_i - T_{i+1})/h_i - \epsilon'_{i-1} \lambda_{i-1} (T_{i-1} - T_i)/h_i \quad \text{for} \quad \epsilon'_i \geq 0, \epsilon'_{i-1} \leq 0, \qquad (12)$$

$$H_i = 0 \quad \text{for} \quad \epsilon'_i \leq 0, \epsilon'_{i-1} \geq 0,$$

where λ_i is a parameter controlling the effective vertical temperature gradient. To make total heat content conservative, λ_i is taken to be 1. Table 2 lists the parameters used in the model.

In order to quantify the performance of the model over the whole model domain, a point by point comparison between model and observations has been carried out by calculating the correlation and the RMS error, as in Miller et al (1993) and Balmaseda et al (1994, 1995). Good correlation skills appear in the equatorial Pacific band of 15°S and 15°N, where the maximum correlation (0.6-0.8) is achieved over a relatively broad area in the central Pacific, decreasing smoothly westward and eastward (Fig.13a). In the RMS error map (Fig.13b), the largest error is located in the eastern Pacific, along the coast of South America. In the remainder of the basin, the RMS error is much smaller, with typical values of 0.4-0.6. Compared with GCMs (Miller et at 1993), the ocean model presented here shares with the GCMs the high RMS error near the South American coast. In the western Pacific the RMS errors are smaller than those in the other models.

Table 3 shows the comparison with other models. In order to allow more direct comparison with the other models, we smoothed our time series by a 5-month running mean filter. The model has generally relatively good correlation skills in the whole equatorial Pacific except in the area of Niño1+2.

Acknowledgements

We are indebted to Dr. D.L.T Anderson and Dr. M.A.Balmaseda for providing their 2-layer model code. This work was supported by grants to W. Hsieh from the Natural Sciences and Engineering Research Council of Canada, and Environment Canada; and by British Council Grant CHI2500134 to K. Haines and Y. Tang.

8 References

Allen, M.R. 1992: Interactions between the atmosphere and ocean on time-scales of weeks to years. *PhD thesis*. University of Oxford, 202 pages.

Anderson, D.L.T, and J.P. McCreary, 1985: Slowly propagating disturbances in a coupled ocean-atmosphere model. *J.Atmos.Sci.,42*, 615-629

Barnston, A.G., and Coauthors, 1994: Long-lead seasonal forecasts-Where do we stand? *Bull. Amer. Meteor.Soc.. 75*, 2097-2114

Balmaseda. M.A, D.L.T. Anderson, and M.K. Davey, 1994: ENSO prediction using a dynamical ocean model coupled to statistical atmospheres, *Tellus, 46(A) 4*, 497-511

——, M.K. Davey, D.L.T. Anderson, 1995: Decadal and seasonal Dependence of ENSO prediction skill. *J. Climate, 8*, 2705-2715

Barnett,T.P., M. Latif, N.E. Graham, M. Flugel, S. Pazan and W. White, 1993: ENSO and ENSO related predictability, Part1: Prediction of equatorial sea surface temperature with a hybrid coupled ocean-atmosphere model. *Climate, 6*, 1545-1566

Battisti, D.S., 1988: Dynamics and thermodynamics of a warming event in a coupled tropical atmosphere-ocean model. *J.Atmos. Sci., 45*, 2889-2919.

Blank,B., J.D. Neelin, and D. Gutzler, 1997: Estimating the effect of stochastic wind stress forcing on ENSO irregularity, *J.Climate,10*,1473-1486

Davey, M.K., S. Ineson, and M.A. Balmaseda, 1994: Simulation and hindcasts of tropical Pacific Ocean interannual variability. *Tellus*, *46A* 433-447

Goldenberg, B. and J.J. O'Brien, 1981: Time and space variability of tropical pacific wind stress, *Mon.Wea.Rev.*, *109*, 1190-1207

Goswami, B.N., and J. Shukla, 1991: Predictability of a coupled ocean-atmosphere model, *J.Climate* , *4*, 3-22.

Hsieh, W.W, and B. Tang, 1998: Applying neural network models to prediction and analysis in meteorology and oceanography. *Bull. Amer. Meteor.Soc.*, *79*, 1855-1870.

Latif, M., T.P. Barnett, M.A. Cane, M. Flugel, N.E. Graham, H.von Storch, J.S.Xu, and S.E.Zebiak, 1994: A review of ENSO prediction studies. *Climate Dyn.*,*9*, 167-179

—–, J. Biercamp, H.von Storch, M.J. McPhaden, and E. Kirk, 1990: Simulation of ENSO-related surface wind anomalies with an atmospheric GCM forced by observed SST. *J.Climate*,*3*,509-521.

—–, M. Flügel, 1991: An Investigation of Short-Range climate predictability in the Tropical Pacific. *J.Geophys.Res*,*96*,2661-2673.

—–, N.E. Graham, 1992: How much predictive skills is contained in the thermal structure of an Oceanic GCM? *J. Phys.Oceanogr.*,*22*, 951-962

—–, A. Villwock, 1990: Interannual variability as simulated in coupled ocean-atmosphere model, *J.Mar.Syst.*, *1*, 51-60

Miller, A.J., T.P. Barnett, and N.E. Graham, 1993: A comparison of some tropical ocean models: Hindcast Skill and El Niño Evolution. *J. Phys. Oceanoger.*, *23*, 1557-1591

Neelin, J.D., 1990: A hybrid coupled general circulation model for El Niño studies, *J.Atmos.Sci.*, *5*, 674-693

Oberhuber, J.M, 1988: An atlas based on COADS dataset: the budgets of heat, buoyancy and turbulence kinetic energy at the surface of the global ocean, Max-Plank-Institute fur Meteorologie, Report No.15

Palmer, T.N, and D.L.T. Anderson, 1994: The prospects for seasonal forecasting -A review paper, *Q.J.Roy.Met.sci.*, *7*, 755-793

Slutz, R. et al 1985: The Comprehensive ocean-atmosphere data set release.I: Climate Research Program, ERL/NOAA, Boulder,CO,39pp.

Stockdale, T.N., 1992: Simulation and prediction of tropical SST with a coupled ocean-atmosphere model, *PhD thesis*, Oxford University, UK

Syu, H.H., J.D. Neelin, and D. Gutzler, 1995: Seasonal and Interannual variability in a hybrid coupled GCM, *J. Climate*, *9*, 2121-2143

Tang, B., W.W. Hsieh, A.H. Monahan, and F.T. Tangang, 1999: Skill comparisions between neural network and canonical correlation analysis in predicting the equatorial Pacific sea surface temperatures, *J. Climate*, submitted.

Tangang, F.T., W.W. Hsieh, and B. Tang, 1998a: Forecasting regional sea surface temperatures of the tropic by neural network models, with wind stress and sea level pressure as predictors. *J. Geophys.Res.*, *103*, 7511-7522

——, B. Tang, and A.H. Monahan, and W.W. Hsieh, 1998b: Forecasting ENSO events: a neural network-extended EOF approach. *J.Climate*,*11*, 29-41

White, W.B., and S.E. Pazan, 1987: Hindcast/forecast of ENSO events based upon the redistribution of observed and model heat content in the western tropical Pacific, 1964-86. *J. Phys. Oceanoger.*, *17*, 264-280

Wu, D-H., D.L.T. Anderson, and M.K. Davey, 1994: ENSO prediction experiments using a simple ocean-atmosphere model. *Tellus*, *49A*, 464-480

Xue, Y., M.A. Cane, S.E. Zebiak and M.B. Blumenthal, 1994: On the prediction of ENSO: a study with a low order markov model. *Tellus*, *46A*, 512-528

Zebiak, S.E.,1989: Oceanic heat content variability and El Niño cycles. *J. Phys. Oceanogr*, *19*, 475-486

Table 1: Correlation between the predicted wind stress EOF time series and the observed wind stress EOF time series for the first 3 modes, using the observed SST, the model HC, the model SST, and the model HC+SST as predictors. Results are shown for both the NN model and the LR model, and for the zonal (x) and meridional (y) components of the wind stress.

Predictors	Obs.SST		HC		Mod.SST		HC+SST	
Predictands	NN	LR	NN	LR	NN	LR	NN	LR
$\tau_x : \beta_1$	0.74	0.72	0.89	0.89	0.81	0.81	0.88	0.88
$\tau_x : \beta_2$	0.57	0.52	0.76	0.73	0.54	0.52	0.75	0.70
$\tau_x : \beta_3$	0.38	0.24	0.40	0.35	0.11	0.06	0.29	0.26
$\tau_y : \beta_1$	0.86	0.83	0.86	0.86	0.83	0.81	0.84	0.86
$\tau_y : \beta_2$	0.53	0.43	0.66	0.66	0.47	0.46	0.57	0.62
$\tau_y : \beta_3$	0.47	0.45	0.24	0.21	0.21	0.19	0.28	0.24

Table 2: Values of the parameters used in the 6-layer ocean model

Layer	$H(m)$	t_e(days)	t_d(days)	$H_{init}(m)$	$T_{init}(^\circ C)$	A
1	100	1	500	100	26	0.75
2	175	150	500*150	175	16	1
3	250	150	500*150	250	13	1
4	320	150	500*150	320	10	1
5	400	150	500*150	400	8	1
6	500	150	500*150	500	6	1

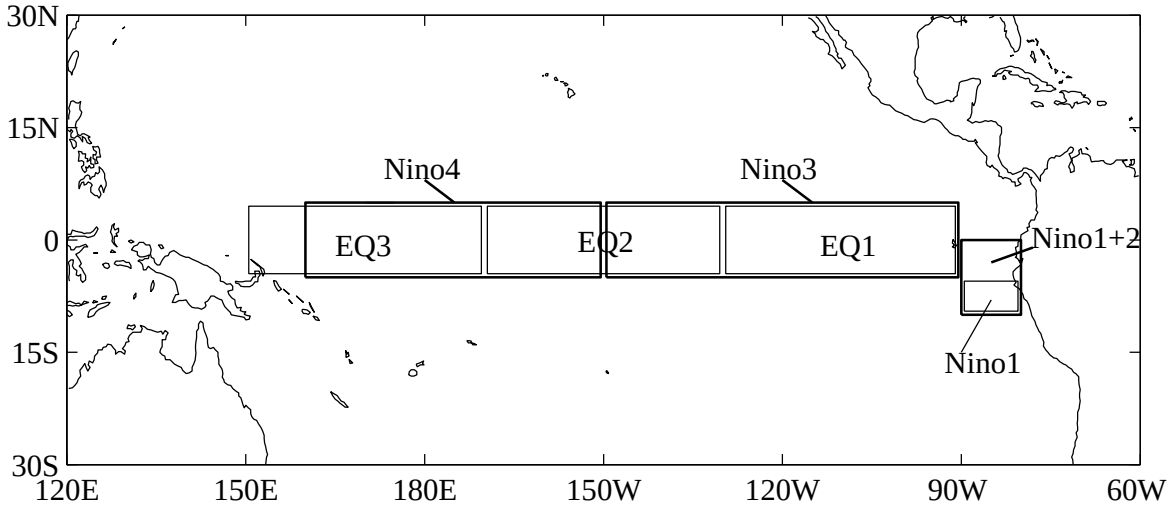

Figure 1: Location of the various oceanic regions used in the analysis.

Table 3: Correlation between the observed SST and that from 10 models. The results of the first 9 models are taken from Palmer and Anderson (1994). The final model is the one used in this study. Model A, described in Wu et al (1994), is a $1\frac{1}{2}$ layer model with specified mean climatology. Model B, is a $2\frac{1}{2}$-layer model, described in Balmaseda et al (1994). Model C, described in Davey et al(1994), is also a $2\frac{1}{2}$-layer model. While model D and E are versions of the GFDL Modular Ocean Model, with resolution of $1\frac{1}{2}^o \times 1\frac{1}{2}^o$ and $\frac{1}{3}^o$ latitude $\times 1\frac{1}{2}^o$ longitude respectively.

Model	Region					
	EQ3	Niño4	EQ2	Niño3	EQ1	Niño1+2
Cane-Zebiak	–	0.46	–	0.60	–	0.68
Max-Planck Institute	–	0.76	–	0.74	–	0.59
OPYC	–	0.72	–	0.63	–	0.46
GFDL	–	0.81	–	0.69	–	0.57
A	0.43	0.64	0.77	0.73	0.69	0.54
B	0.27	0.59	0.77	0.75	0.69	0.40
C	0.34	0.55	0.67	0.62	0.51	0.26
D	0.60	0.76	0.79	0.55	0.55	0.54
E	0.59	0.76	0.79	0.65	0.60	0.58
Model used here	**0.55**	**0.73**	**0.82**	**0.80**	**0.75**	**0.38**

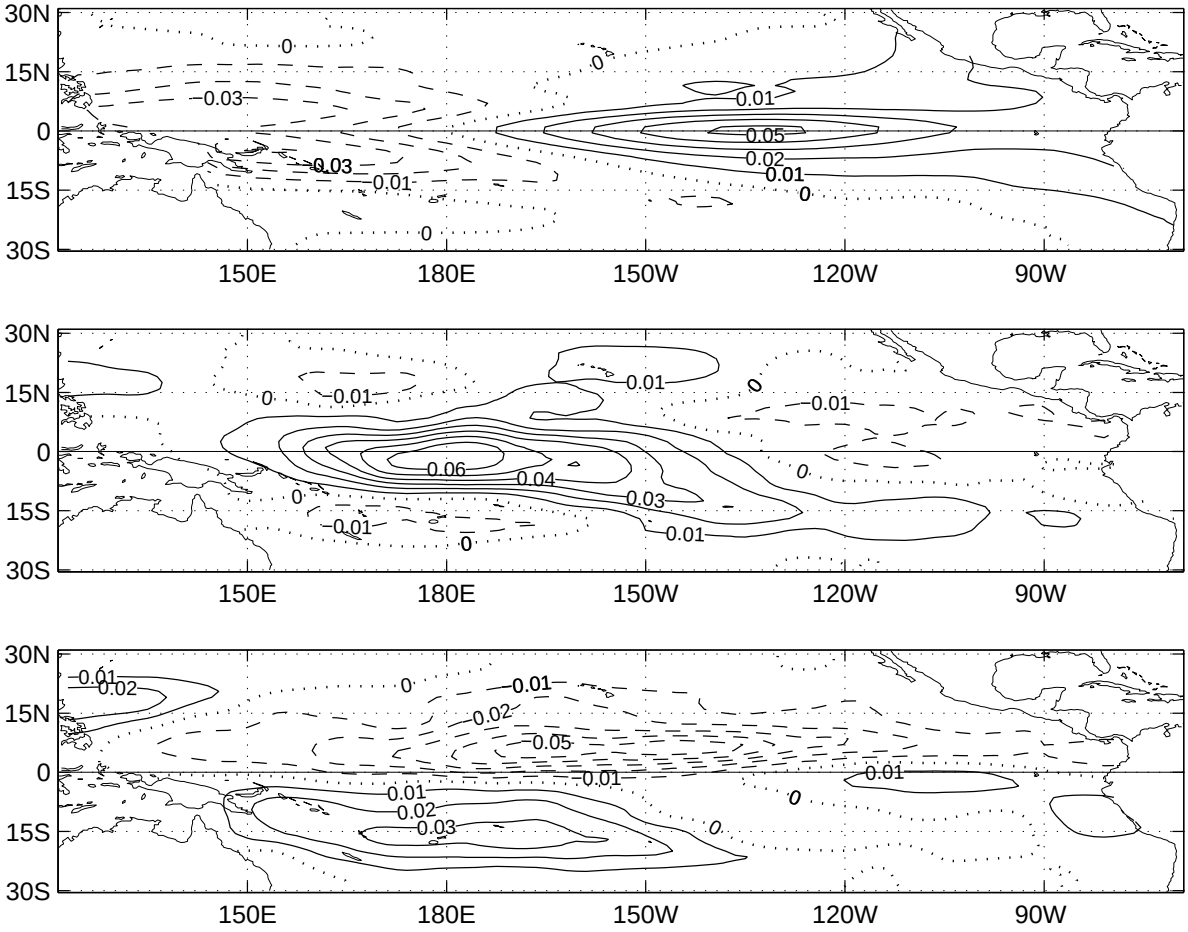

Figure 2: The first EOF mode for (a) the upper ocean heat content (HC) from the ocean model driven by the FSU wind stress, (b) the FSU zonal wind stress and (c) the meridional wind stress. Negative contours are shown as dashed curves and zero contours as dotted curves. (C.i. $= 0.01^{o}$C).

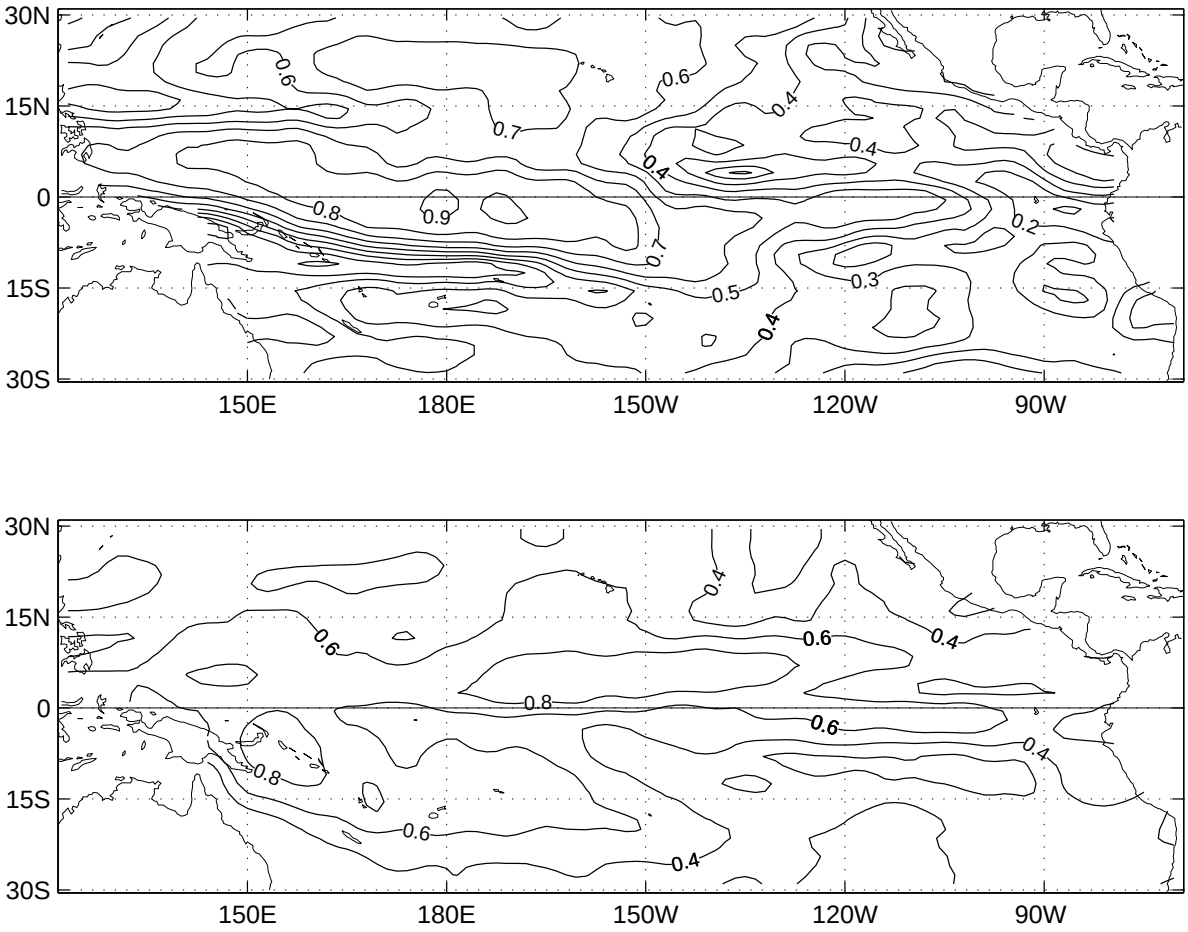

Figure 3: Correlations of the FSU wind stress and the idealized wind stress (reconstructed from the first 3 EOF modes of the FSU wind stress) for (a) the zonal stress (contour interval = c.i. = 0.1), and (b) the meridional stress (c.i. = 0.2).

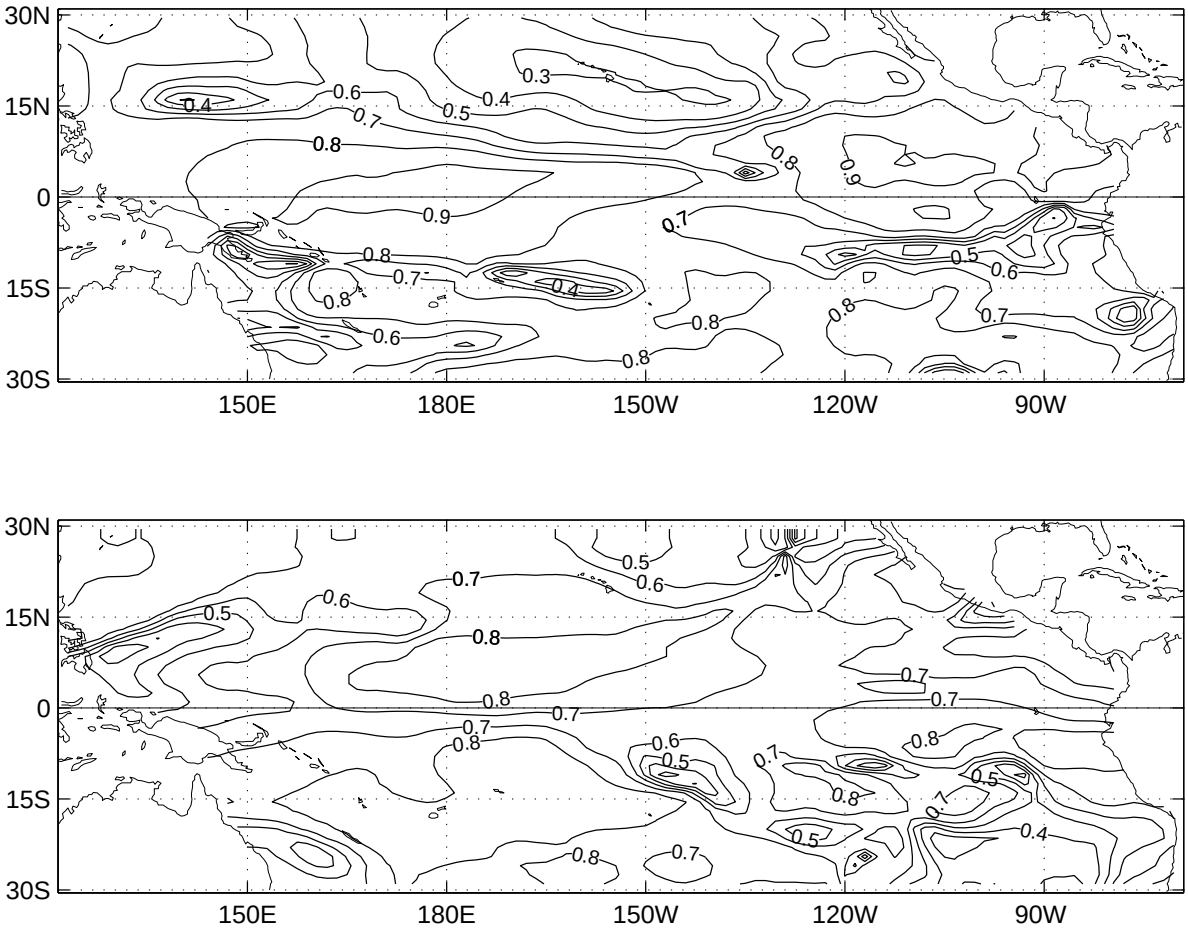

Figure 4: Cross-validated anomaly correlation between the predicted wind stress by NN (with model HC as predictors) and the idealized wind stress (i.e. the FSU wind stress with only the first 3 EOF modes): (a) zonal stress, and (b) meridional stress. C.i.=0.1

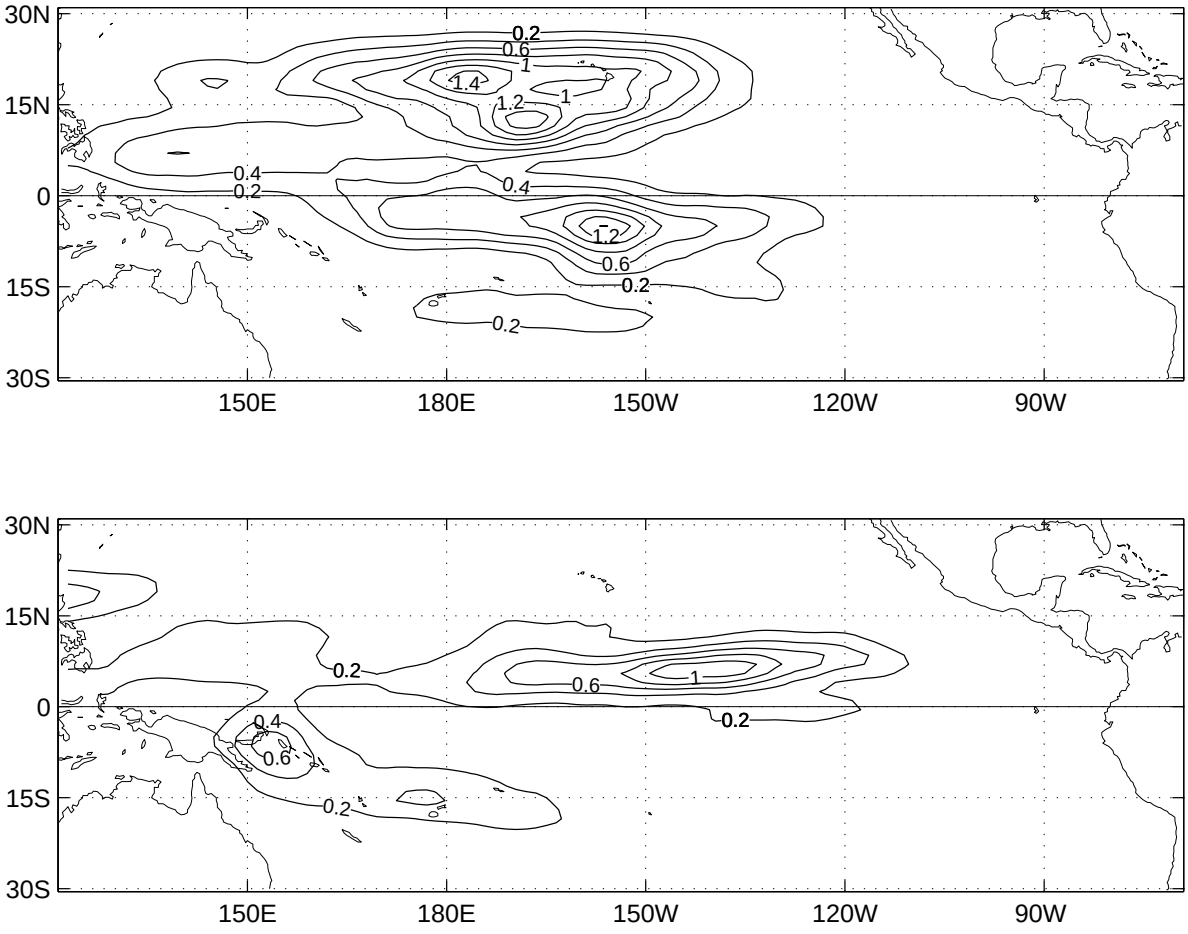

Figure 5: RMS error of the predicted wind stress by NN verified against the idealized wind stress: (a) zonal stress, and (b) meridional stress. C.i.=0.2 N m^{-2}.

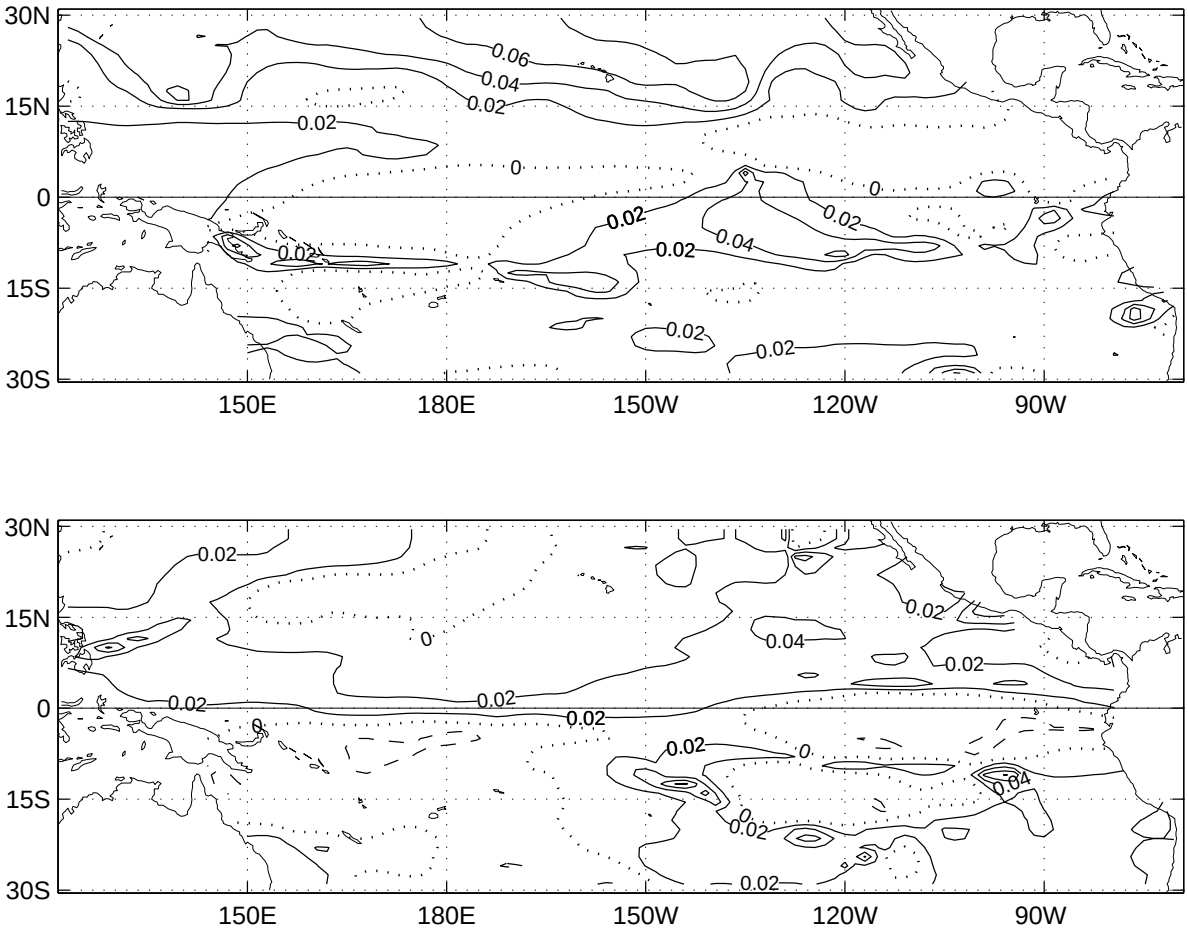

Figure 6: The correlation between the wind stress predicted by the NN model and the idealized stress minus the correlation between the wind stress predicted by the LR model and the idealized wind stress, for: (a) zonal stress, and (b) meridional stress. C.i. = 0.02. The zero contours are the dotted curves, while the negative contours are the dashed curves. Positive values means the NN predicted wind stress is outperforming the LR one.

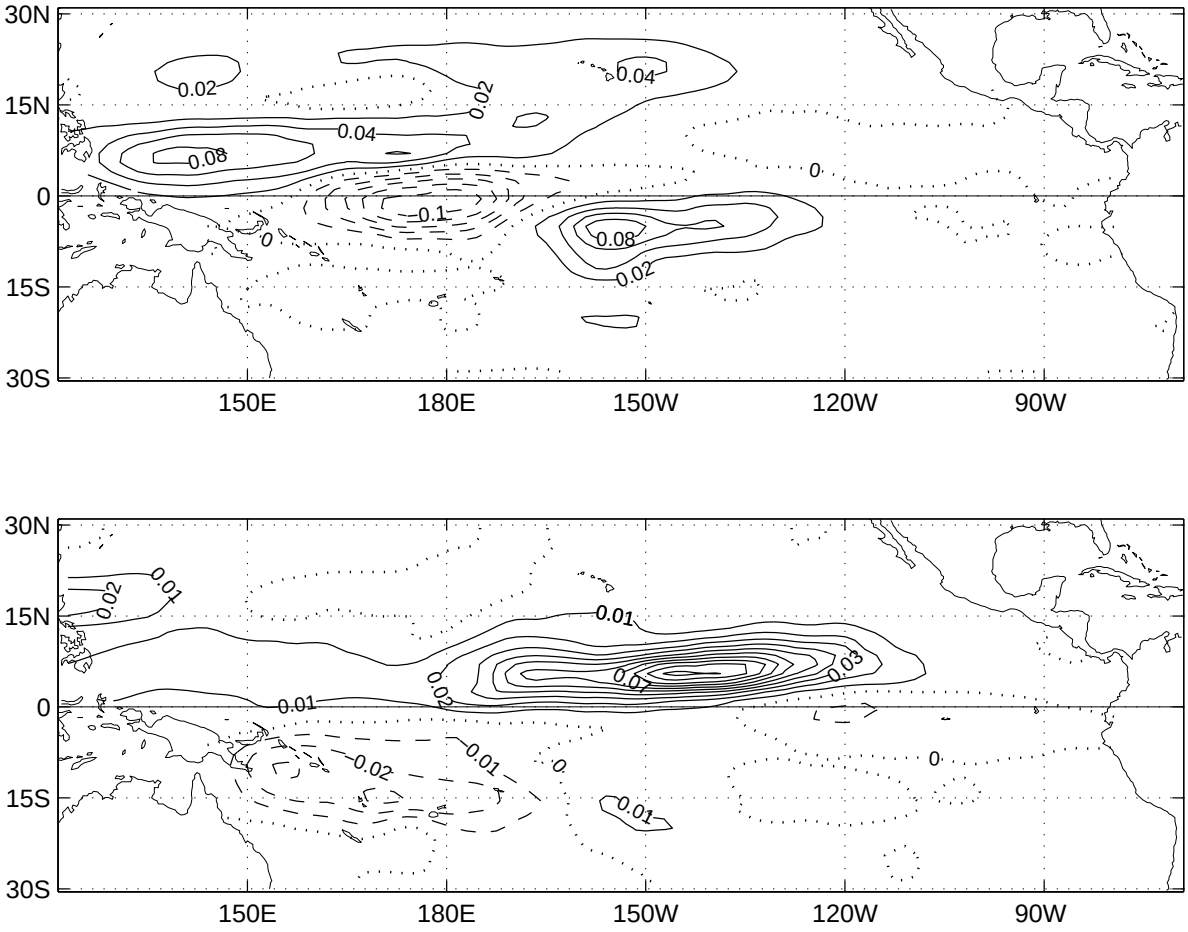

Figure 7: The RMS error of the LR wind stress minus the RMS error of the NN wind stress, (both verified against the idealized wind stress), for: (a) zonal stress, and (b) meridional stress. C.i.=0.02 N m^{-2}. Positive values means the NN predicted wind stress is outperforming the LR one.

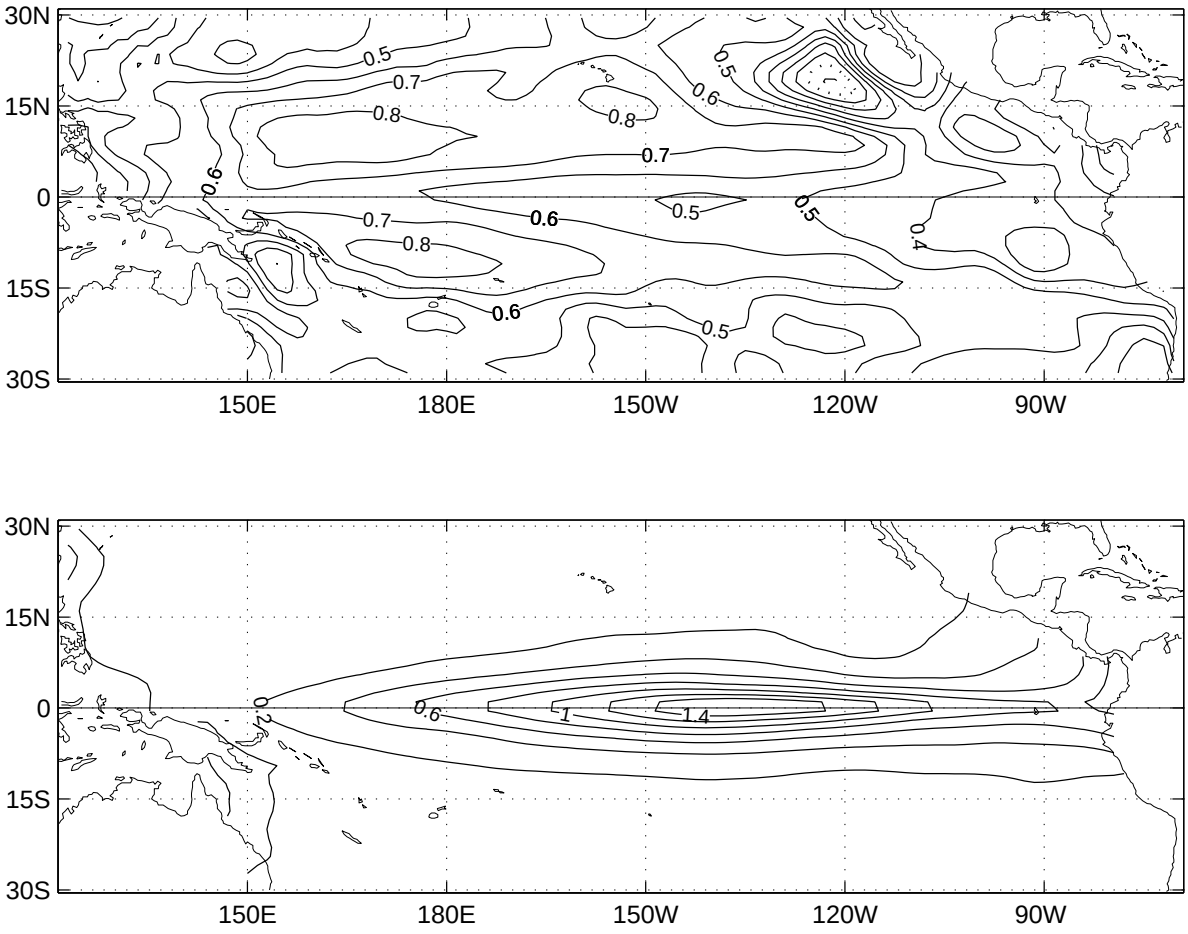

Figure 8: A cross-validated comparison of the model SST between the ocean model driven by the FSU wind stress and that driven by the idealized stress (i.e. with only the first 3 EOFs), by (a) correlation (c.i.=0.1), and (b) RMS error (c.i.=0.2°C).

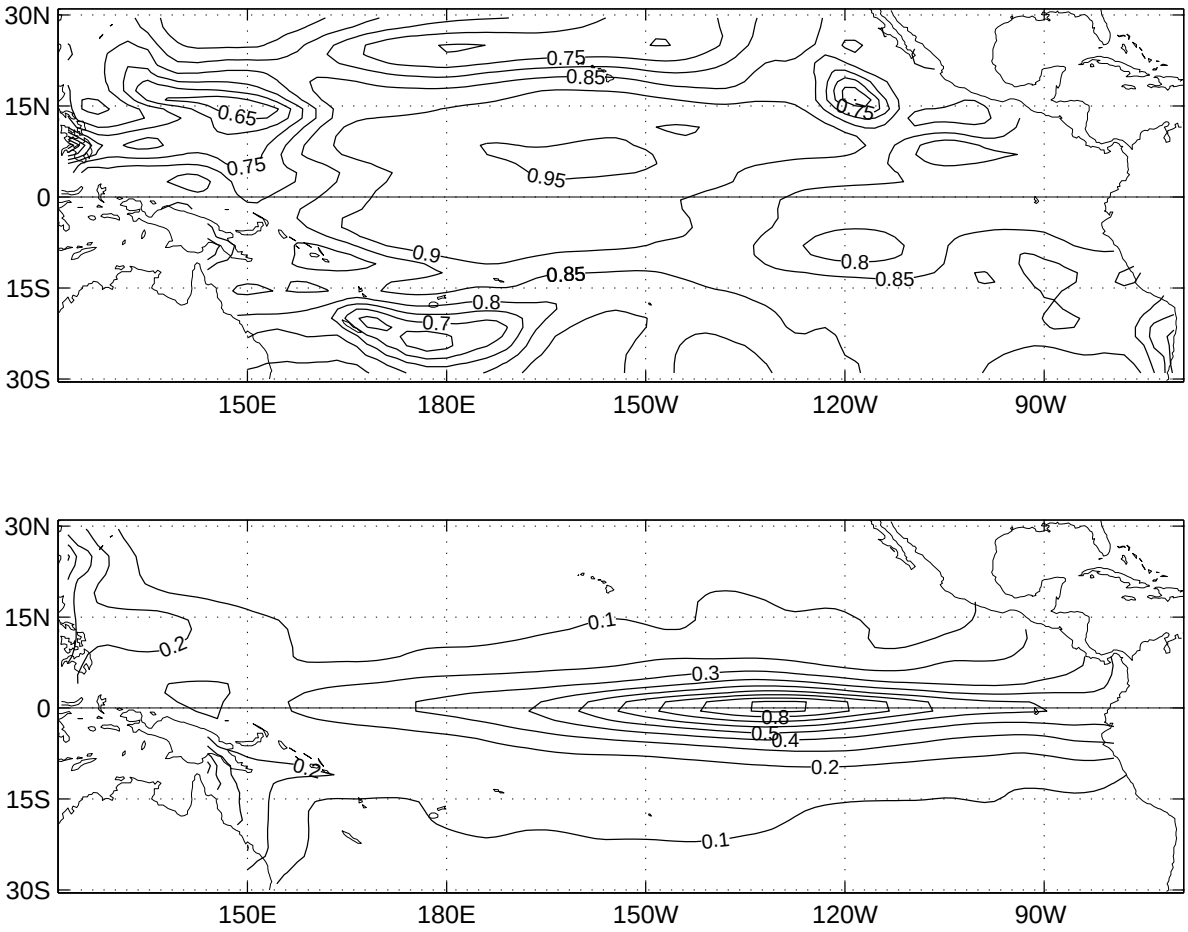

Figure 9: A cross-validated comparison of the ocean model SST between that driven by the idealized wind stress and that driven by the empirical wind stress from the NN model (with HC as predictors), by (a) correlation (c.i.=0.05), and (b) RMS error (c.i.=0.1°C).

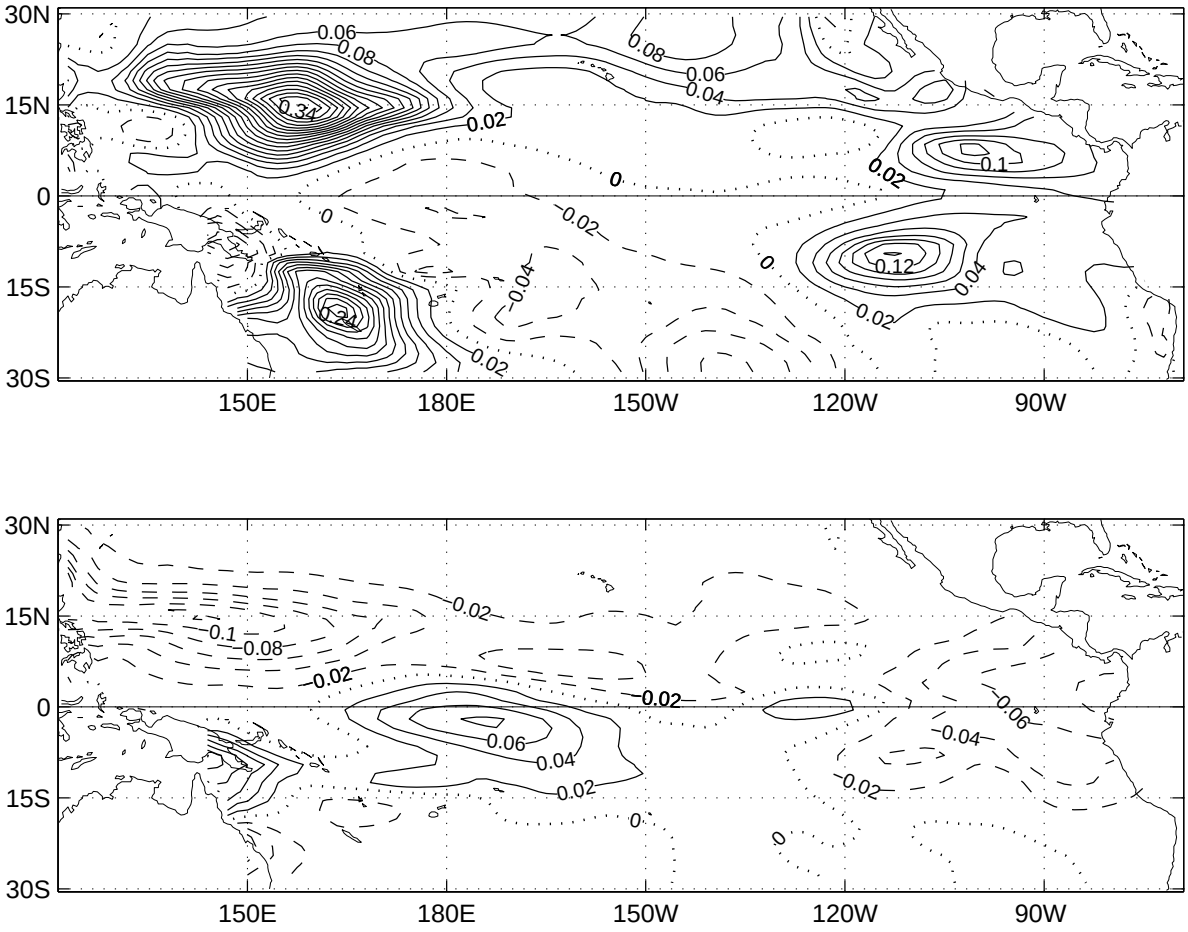

Figure 10: The skill differences in the model SST between the model driven by the NN model wind stress and that driven by the LR model stress, with both model SSTs verified against the standard SST, i.e. the modby the idealized wind stress: (a) correlation skill difference (c.i. = 0.02), and (b) RMS error difference (c.i.=0.02°C). Positive regions in (a) indicate NN ahead of LR, while negative region in (b) indicate NN ahead of LR.

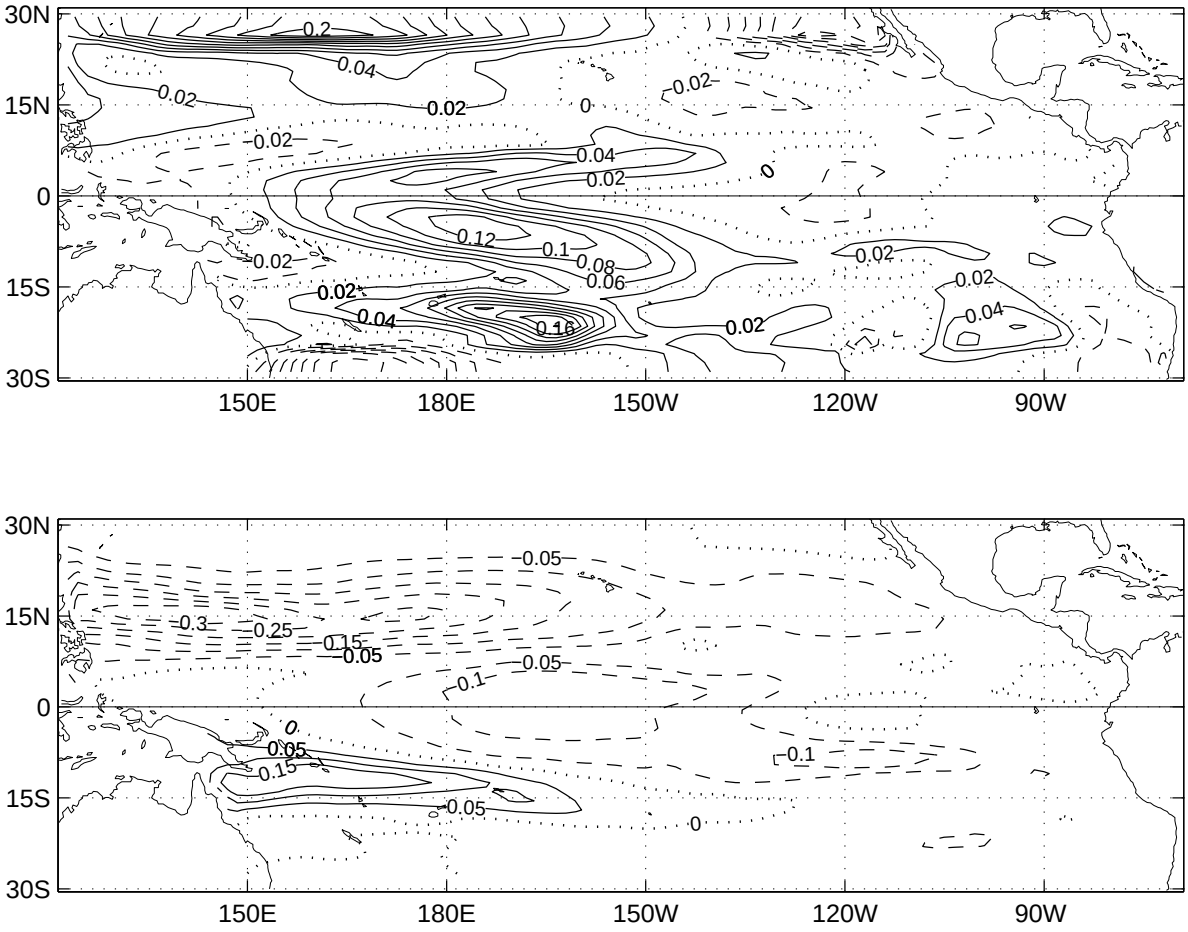

Figure 11: Cross-validated skill differences in the model HC between the ocean model driven by NN model wind stress and that driven by the LR model stress, both verified against the model HC driven by the idealized wind stress: (a) correlation difference (c.i. = 0.02), (b) RMS error difference (c.i.=0.05°C). Positive regions in (a) indicate NN ahead of LR, while negative regions in (b) indicate NN ahead of LR.

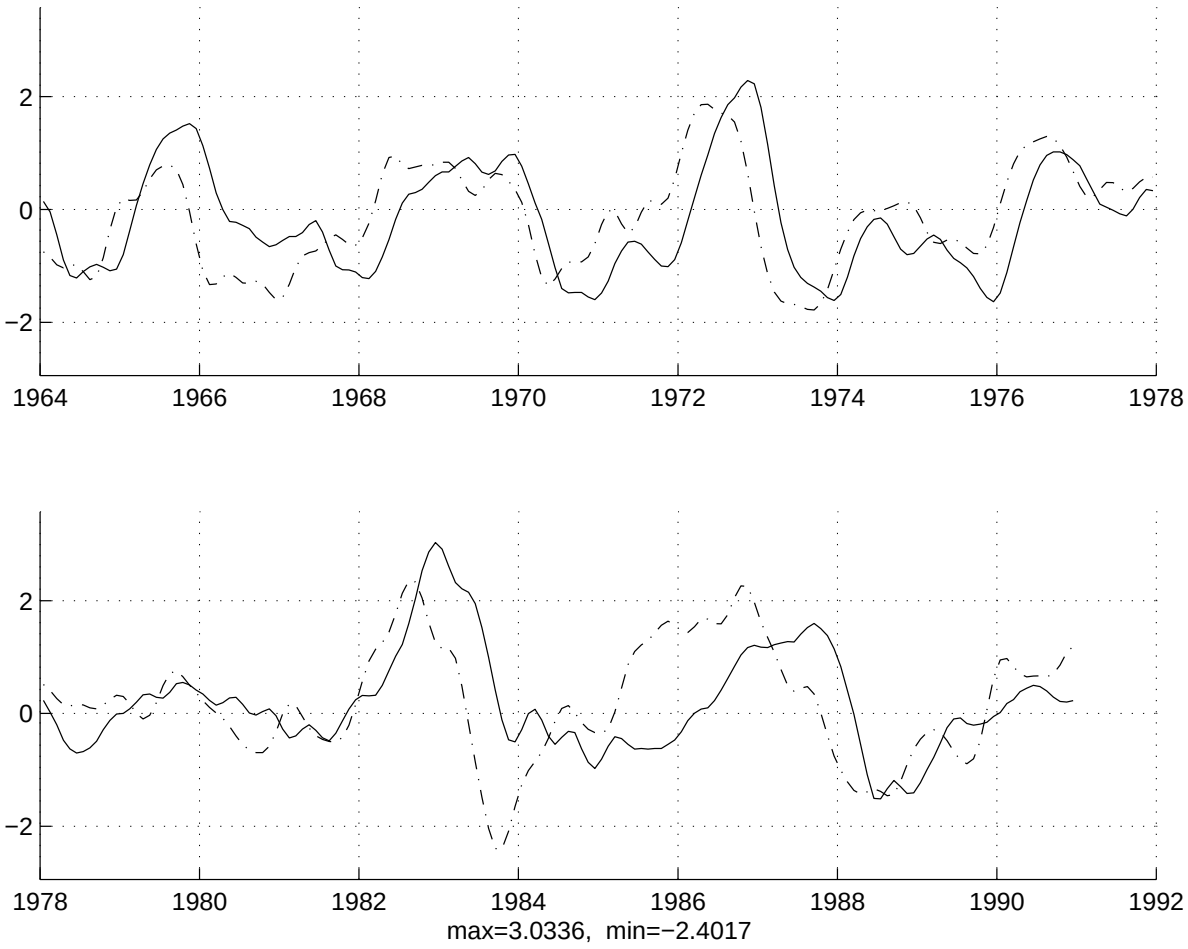

Figure 12: Time evolution of observed SST anomalies in NINO3 and model upper HC forced FSU observed wind stress in whole equatorial equatorial Pacific (124°E-70°W,5°N-5°S). Both were normalised and smoothed by 3 point running mean. Solid line is for SST and dash line for HC.

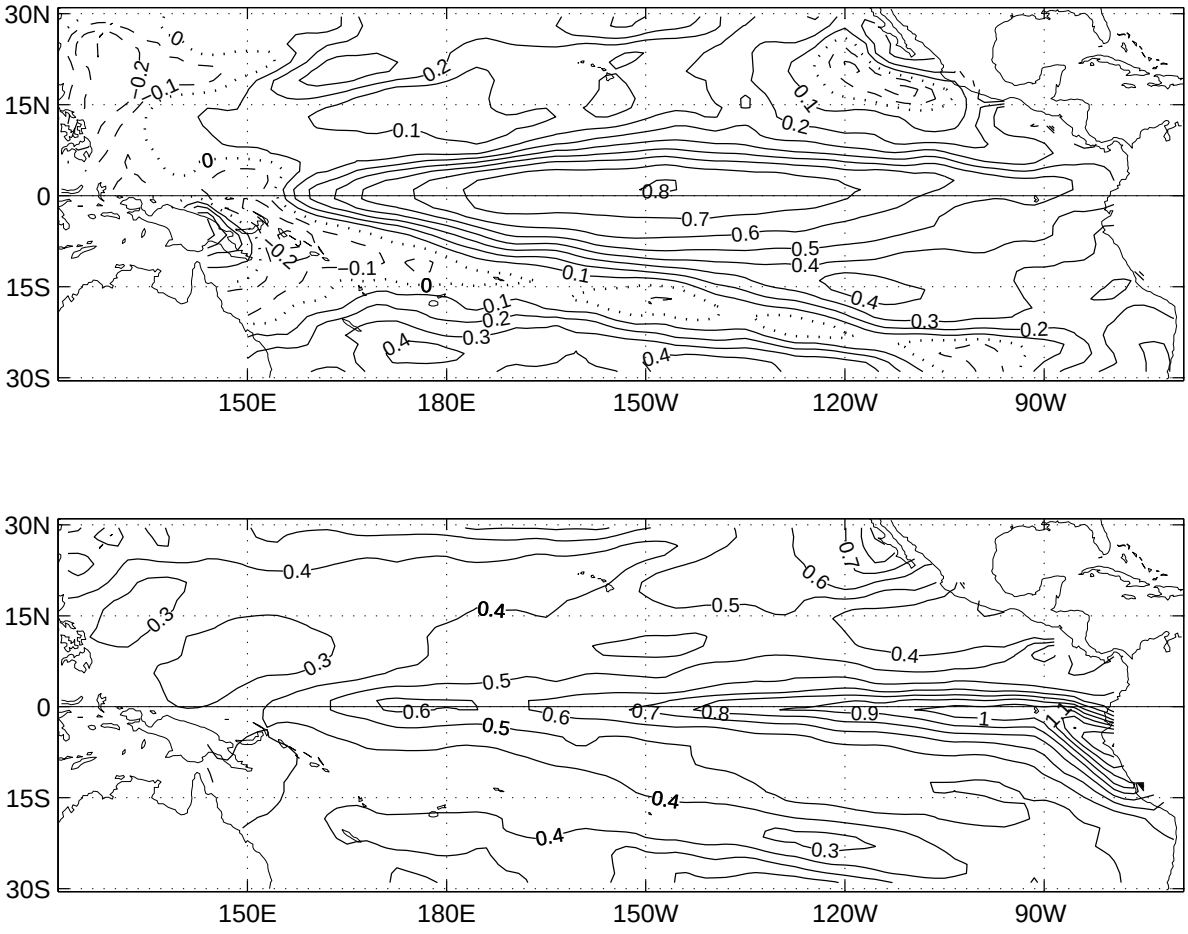

Figure 13: Statistics for the model SST anomalies relative to the COADS SST data: (a) correlation (c.i.=0.1) and (b) RMS error (c.i.=0.1^{o}C).